RSC Advances

PAPER

Cite this: *RSC Adv.*, 2024, **14**, 12864

Rational design of a lysosome-targeted fluorescent probe for monitoring the generation of hydroxyl radicals in ferroptosis pathways†

Lili Zhong,‡[a] Datian Fu,‡[b] Jin Xu,[c] Linyan Tan,[d] Haimei Wu *[e] and Min Wang[a]

Received 22nd January 2024
Accepted 25th March 2024

DOI: 10.1039/d4ra00562g

rsc.li/rsc-advances

Ferroptosis is a newly discovered iron-dependent form of regulated cell death associated with high levels of hydroxyl radical (˙OH) production. Meanwhile, lysosome dysfunction has been shown to be one of the causes of ferroptosis. Although a variety of ˙OH-responsive fluorescent probes have been developed for detecting intracellular ˙OH in living cells, there are still only few lysosome-targeted probes to monitor the variation in lysosomal ˙OH levels during ferroptosis. Herein, we report a novel ˙OH-specific fluorescent probe HCy-Lyso, which is composed of the hydrocyanine and morpholine moiety. Upon treatment with ˙OH, its hydrocyanine unit was converted to the corresponding cyanine group, thus leading to a large π-conjugation extension of HCy-Lyso, accompanied by a significant fluorescence off–on response. Moreover, after reacting with ˙OH in an acidic environment, the protonation product of HCy-Lyso exhibits a higher fluorescence enhancement, which is suitable for detecting lysosomal ˙OH variation. HCy-Lyso has been utilized for imaging endogenous ˙OH in living cells under phorbol myristate acetate (PMA) stimuli and monitoring the changes in lysosomal ˙OH levels during ferroptosis. Thus, our study proposes a new strategy to design lysosome-targeted and ˙OH-responsive fluorescent probes to investigate the relationship between lysosomes and ferroptosis.

1 Introduction

Ferroptosis, a unique cell death pathway proposed by Stockwell and co-workers in 2012,[1,2] is closely related to various diseases, such as neurodegeneration, acute lymphoblastic leukemia, ischemic reperfusion injury, autoimmune diseases and so on.[3–7] Owing to its pathological functions and potential in tumor therapeutics, ferroptosis has attracted widespread attention in the past few years.[8] The detection of ferroptosis and its associated signaling molecules is essential for monitoring the ferroptosis process and evaluating ferroptosis-related therapies. It has been revealed that the hydroxyl radical (˙OH), one of the most active reactive oxygen species (ROS), is observed to be markedly generated during the programmed death process of ferroptosis.[9] Intracellular ˙OH is mainly produced *via* the transition metal iron-participating Fenton reaction, which catalyzes the ferrous iron (Fe^{2+}) and hydrogen peroxide (H_2O_2) in the acidic environment of cells, which further causes the lethal lipid peroxidation because of its strong hydrogen abstraction ability.[10,11] Therefore, detecting and quantifying intracellular ˙OH levels is crucial for deeply understanding the modulation mechanisms and pathological functions of ferroptosis, which, however, is still a challenge. It is of great importance to develop a new and efficient method for sensitively and selectively detecting ˙OH in biological systems.

Lysosomes, some of the most promising organelle targets, play important roles in several metabolic processes, such as cellular apoptosis, plasma membrane repair, immunological stress, energy metabolism and autophagy.[12–16] Recent studies have reported that lysosomes execute a broad range of functions in cellular metal homeostasis by regulating the inter-compartmental fluxes, redox states, storage and detoxification of metal ions.[17–20] Moreover, accumulating evidence suggest that lysosomes are not only participants in the autophagy process, but also vital iron storage hubs in cells.[21–26] For instance, ferritinophagy, the autophagic degradation of ferritin, triggers the release of iron in lysosomes.[27] Moreover, lysosomal dysfunction can induce lysosomal membrane permeabilization (LMP), resulting in the release of considerable iron into the cytoplasm, further enhancing cell-intrinsic Fenton chemistry.[28–30] Therefore, monitoring ˙OH generation and

[a]*Department of Pharmacy, Hainan General Hospital (Hainan Affiliated Hospital of Hainan Medical University), Haikou, Hainan, 570311, China*
[b]*Department of Pharmacy, Hainan Women and Children's Medical Center, Haikou, Hainan, 570312, China*
[c]*Pharmaceutical and Bioengineering School, Hunan Chemical Vocational Technology College, Zhuzhou, 412006, China*
[d]*Department of Pharmacy, Tropical Agricultural Technology College, Hainan Vocational University, Haikou, Hainan, 570216, China*
[e]*Department of Clinical Pharmacy, Hainan Cancer Hospital, Haikou, Hainan, 570100, China. E-mail: wu634202863@126.com*

† Electronic supplementary information (ESI) available. See DOI: https://doi.org/10.1039/d4ra00562g

‡ These authors contribute equally to this work.

dynamics in lysosomes is particularly important to gain insights into the ferroptosis process. Fluorescent probes have been widely used for the sensitive, selective and noninvasive imaging of bioactive species.[31–37] To date, a variety of fluorescent probes have been prepared to detect and monitor ˙OH levels in the cellular microenvironment, which are mainly based on the oxidation or aromatic hydroxylation ability of ˙OH.[38–45] Besides, tracking the ˙OH fluctuation in sub-organelles can provide more information for deeply understanding the mechanism of ferroptosis pathways. Numerous mitochondria or nucleoli targeted ˙OH fluorescent probes were further synthesized and used for imaging the subcellular ˙OH changes.[46] However, most of these probes do not display lysosome-targeting ability and cannot accurately detect the lysosomal ˙OH in cells. Thus, it is still meaningful to develop a novel fluorescent probe for detecting the lysosomal ˙OH level during ferroptosis.

Herein, we report a novel lysosome-targeting, hydrocyanine-based turn-on fluorescent probe (denoted as HCy-Lyso) for monitoring changes in lysosomal ˙OH (Scheme 1). HCy-Lyso is a hybrid compound of the hydrocyanine and the morpholine moiety, in which the hydrocyanine unit acts as the ˙OH recognition site and the morpholine group of HCy-Lyso afford specificity to lysosomes. In the beginning, HCy-Lyso itself is almost nonfluorescent in an aqueous solution, which is mainly attributed to the small π-conjugation and coplanarity. However, upon treatment with ˙OH, it formed a larger π-conjugation of cyanine (HCy-OH), thus leading to a significant fluorescence recovery at 598 nm. Notably, HCy-Lyso exhibits a stronger fluorescence intensity when it reacts with ˙OH in an acidic environment, which is suitable for detecting the change of lysosomal ˙OH. This phenomenon is further confirmed by density-functional theory (DFT) calculations. HCy-Lyso has been successfully utilized for imaging endogenous ˙OH production in living cells under phorbol myristate acetate (PMA) stimuli, as well as detecting the variation of lysosomal ˙OH levels in two different ferroptosis pathways, respectively.

2 Experimental section

2.1 Materials and instruments

All reagents and solvents used for the synthesis were acquired from commercial sources and used without further purification. 4-Morpholinobenzaldehyde (AR, 97%), tetrachloro-1,4-benzoquinone (TCBQ, 98%), phorbol 12-myristate 13-acetate (PMA, 98%), erastin (AR, 99%), and (1*S*,3*R*)-RSL3 (RSL3, 98%) were bought from Macklin Co., Ltd. Ethanol (EtOH, 99.8%) and dimethyl sulfoxide (DMSO, 99.9%) were purchased from Aladdin Chemistry Co., Ltd. LysoTracker Blue DND-22 was ordered from Thermos Fisher Scientific (Invitrogen). Calcein-AM/PI detection kit and Hoechst 33342 were supplied by Beyotime Institute of Biotechnology (Shanghai, China). Cell Counting Kit-8 (CCK-8) assay kit and ferrostatin-1 (Fer-1) were acquired from GlpBio Technology Inc. Roswell Park Memorial Institute 1640 medium (RPMI-1640), trypsin–EDTA, penicillin–streptomycin, and Fetal bovine serum (FBS) were provided by Biological Industries Co., Ltd.

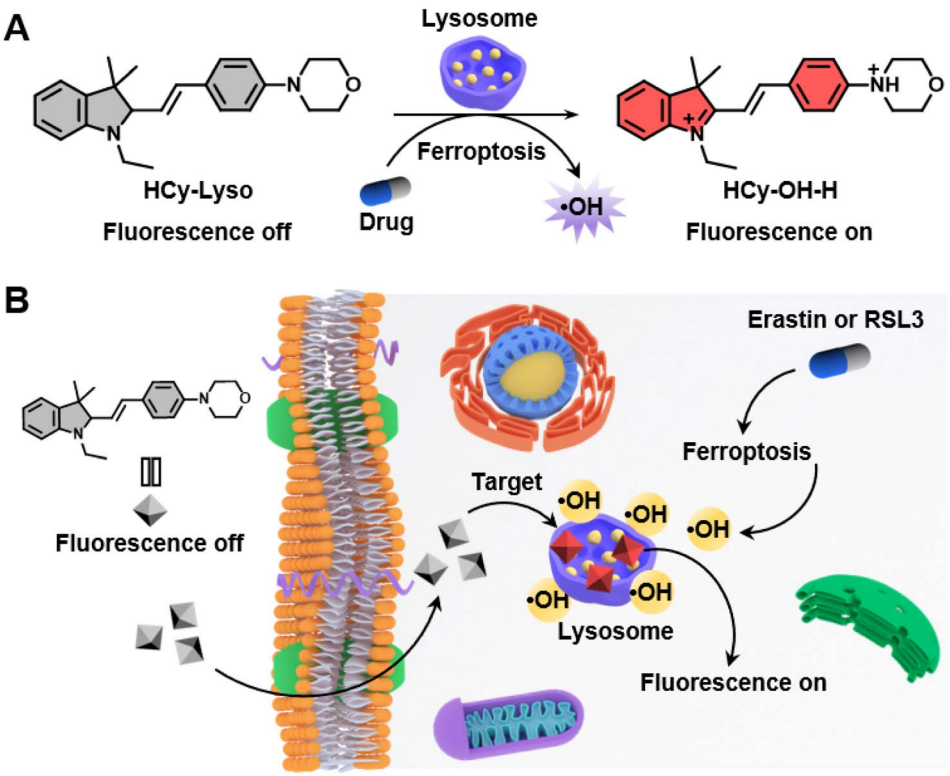

Scheme 1 (A) Chemical structure and fluorescence response mechanism of HCy-Lyso to ˙OH. (B) Schematic illustrations of HCy-Lyso for monitoring the variation in lysosomal ˙OH levels in two different ferroptosis pathways.

^{1}H nuclear magnetic resonance (^{1}H NMR) and ^{13}C NMR were measured in $CDCl_3$ or DMSO-d_6 with tetramethylsilane (TMS) as an internal reference. The NMR spectra data were recorded on a Bruker Avance III 500 spectrometer. High-resolution mass spectra (HRMS) were recorded on a Thermo Scientific mass spectrometer system (Q Exactive) using electrospray ionization (ESI) mode. IR spectra were recorded on a Thermo Scientific Nicolet iS50 infrared spectrometer. Absorption and fluorescence emission spectra were obtained on a UV-3600 spectrophotometer (Shimadzu) and a Hitachi F4700 fluorescence spectrometer, respectively. Cytotoxicity assays were conducted by a Tecan Spark microplate reader. The cell imaging experiments were performed on an inverted fluorescence microscope (Carl Zeiss, Axio Observer A1).

2.2 Synthesis of HCy-OH

Indole salt derivative (compound **1** in Scheme S1†) was first prepared using the reported methods.[47] Then, the solution of 15 mL anhydrous ethanol containing compound **1** (400 mg, 1.27 mmol) and 4-morpholinobenzaldehyde (267 mg, 1.40 mmol) was stirred under reflux at 80 °C for 12 h. After cooling to room temperature, the solvent was evaporated in a vacuum, and the crude product was purified by silica gel chromatography (200–300 mesh) using CH_2Cl_2/CH_3OH (20 : 1, v/v) as the eluent to obtain HCy-OH as a dark red solid (350 mg, 56% yield). m.p. 259.3–265.2 °C. ^{1}H NMR (500 MHz, DMSO-d6) δ 8.37 (d, J = 15.8 Hz, 1H), 8.15 (d, J = 9.0 Hz, 2H), 7.81 (dd, J = 17.0, 7.6 Hz, 2H), 7.55 (tdd, J = 8.0, 7.6, 0.9 Hz, 2H), 7.38 (d, J = 15.8 Hz, 1H), 7.12 (d, J = 9.2 Hz, 2H), 4.60 (q, J = 7.1 Hz, 2H), 3.81–3.70 (m, 4H), 3.57–3.46 (m, 4H), 1.77 (s, 6H), 1.41 (t, J = 7.2 Hz, 3H). ^{13}C NMR (125 MHz, DMSO-d6) δ 180.18, 155.07, 154.91, 143.61, 141.10, 134.40, 129.39, 128.51, 124.41, 123.41, 114.37, 113.86, 106.63, 66.26, 55.41, 51.75, 46.82, 41.41, 26.68, 13.84. IR (KBr): 2964 w, 2851 w, 1570 s, 1522 s, 1469 w, 1365 m, 1323 w, 1298 s, 1237 s, 1190 s, 1115 m, 1085 w, 1046 w, 1017 w, 921 m, 824 m, 765 m, 700 m, 632 m, 588 w, 491 2. HRMS (ESI) m/z calculated for $C_{24}H_{29}N_2O^+$ $[M]^+$: 361.2275, found: 361.2340.

2.3 Synthesis of HCy-Lyso

HCy-OH (100 mg, 0.2 mmol), $NaBH_4$ (7.8 mg, 0.2 mmol), and 10 mL of anhydrous ethanol were added into a 25 mL three-neck round-bottomed flask. Then, the mixture was stirred at room temperature under nitrogen for 10 min. After removing the solvent under reduced pressure, the residue was purified by silica gel column chromatography (CH_2Cl_2/CH_3OH, 20 : 1, v/v) to give HCy-Lyso as a pink solid (39 mg, 53% yield). m.p. 161.3–164.5 °C. ^{1}H NMR (500 MHz, $CDCl_3$) δ 7.40–7.35 (m, 2H), 7.09 (td, J = 7.7, 1.3 Hz, 1H), 7.02 (dd, J = 7.2, 1.0 Hz, 1H), 6.92–6.87 (m, 2H), 6.70 (td, J = 7.4, 0.8 Hz, 1H), 6.57 (d, J = 15.8 Hz, 1H), 6.50 (d, J = 7.7 Hz, 1H), 6.12 (dd, J = 15.8, 9.2 Hz, 1H), 3.91–3.83 (m, 4H), 3.69 (d, J = 9.2 Hz, 1H), 3.31 (dq, J = 14.3, 7.1 Hz, 1H), 3.20–3.16 (m, 4H), 3.13 (dt, J = 17.1, 7.0 Hz, 1H), 1.30 (s, 3H), 1.08 (s, 3H), 1.05 (t, J = 7.1 Hz, 3H). ^{13}C NMR (125 MHz, $CDCl_3$) δ 150.87, 149.69, 139.14, 133.46, 128.73, 127.45, 124.98, 121.82, 117.50, 115.57, 107.22, 66.85, 53.46, 49.16, 44.32, 39.67, 25.86, 24.18, 10.39. IR (KBr): 3028 w, 2966 m, 2926 w, 2844 m, 1646 w, 1603 s, 1515 s, 1479 s, 1451 m, 1370 m, 1341 w, 1305 w, 1266 s, 1225 s, 1173 w, 1120 s, 1053 w, 1020 w, 979 w, 927 m, 859 w, 812 s, 752 s. HRMS (ESI) m/z calculated for $C_{24}H_{30}N_2O$ $[M + H]^+$: 363.2436, found: 363.2484.

2.4 General procedures for spectral measurements

Unless otherwise mentioned, the stock solution of HCy-Lyso (1 mM) was prepared in DMSO, and all spectral measurements were carried out in 10 mM PBS buffer at 37 °C. Typically, 20 μL of HCy-Lyso stock solution (final concentration of 10 μM) was added to the test tubes containing 2.0 mL of PBS solution with different pH (4.0–7.4), followed by introducing an appropriate volume of TCBQ/H_2O_2. The mixed solution was allowed to react at 37 °C for 1.0 h before absorption or fluorescence measurements. Note: the TCBQ solution was added to a mixture of H_2O_2 in pH 7.4 or 4.0 phosphate buffer to generate $^{\bullet}$OH, and the molar concentration of $^{\bullet}$OH was equal to the TCBQ/H_2O_2 molar concentration.

2.5 Fluorescence quantum yield (QY) measurement

The QY of HCy-Lyso and HCy-Lyso treated with TCBQ/H_2O_2 in pH 4.0 PBS solution was determined from the relative fluorescence quantum yields by comparing with the RhB dye (QY = 0.97 in EtOH) as the reference. Five different concentrations were measured and the integrated fluorescence intensity (525–800 nm) was plotted against the absorbance value at the corresponding excitation wavelength (510 nm) for all the samples. The quantum yield was calculated in the following manner:

$$QY_s = QY_r \times (slope_s/slope_r) \times (n_s/n_r)^2 \quad (1)$$

where subscripts s and r denote the sample and reference, respectively; n is the refractive index of the solvent. The absorbance of all samples is carefully controlled to lower than 0.1 in 510 nm for all measurements to eliminate the self-quenching phenomenon.

2.6 Theoretical calculations

All three molecules (HCy-Lyso, HCy-OH, and HCy-OH-H) were fully optimized with the density functional theory (DFT) and time-dependent density functional theory (TD-DFT) method using the B3LYP-D3 density functional, which is one of the most commonly used in the published literature for studying the structural properties of organic molecules.[48,49] B3LYP-D3 functional can also achieve a remarkable improvement in the accuracy of calculated results compared to the standard B3LYP functional. Besides, the 6-311G(d) basis set is carefully selected to obtain the best concordance with the experimental results.[50] Analytical frequency calculations were performed at the same level of theory to confirm that the optimized ground-state and excited-state structures were at a minimum point, and the emission energies of all molecules were subsequently calculated. The solvent (H_2O) effect was included in all calculations using the solvation model based on the density (SMD). The above quantum chemical calculations were carried out by using the Gaussian 16 program.[51]

2.7 Cell culture and cytotoxicity assay

Murine breast cancer cell (4T1) was obtained from the Institute of Basic Medical Sciences (IBMS) of the Chinese Academy of Medical Sciences. Cells were grown in RPMI-1640 culture medium containing 10% FBS and 1% antibiotics (penicillin–streptomycin) at 37 °C in a humidified environment of 5% CO_2. The cytotoxicity was measured using a standard CCK-8 assay. Typically, 4T1 cells were seeded on a 96-well plate at a density of 3.5×10^3 cells per well and incubated for 24 h. Then, 100 μL fresh culture medium containing HCy-Lyso with different concentrations (0, 0.6, 1.3, 2.5, 5.0, and 10 μM) was added to the wells. After culturing for another 12 h, the media were removed and washed with PBS three times. Cells were then incubated with fresh RPMI-1640 medium containing 10% CCK-8 for 2 h in the dark. Finally, the absorbance of the products was measured at a wavelength of 450 nm by a microplate reader.

2.8 Live-dead cell staining

4T1 cells (3.5×10^3 cells per well) were seeded in a 96-well plate to adhere for 24 h. After reaching 80% confluence, the cells were treated with various concentrations of HCy-Lyso (0, 2.5, 5.0, and 10 μM) at 37 °C for 12 h. Then, cells were successively stained with calcein-AM and propidium iodide (PI) for 30 min in the dark. Finally, the fluorescence images were immediately obtained using an inverted fluorescence microscope.

2.9 Subcellular colocalization assay

In brief, 4T1 cells were first incubated on 96-well plates at a density of 2.5×10^3 cells per well for 24 h. HCy-Lyso (10 μM) was then added into wells and co-incubated for 0.5 h. Subsequently, the cells were gently washed with PBS three times, followed by adding 100 μL of LysoTracker Blue DND-22 (75 nM) dyeing solution for another 30 min at 37 °C. The red and blue fluorescence in the wells were observed by an inverted fluorescence microscope.

2.10 Fluorescence imaging of ˙OH in 4T1 cells under PMA stimuli

4T1 cells (2.5×10^3 cells per well) were randomly seeded in 96-well plates and incubated for 24 h at 37 °C. Then, the cells were treated with PMA (2.0 μg mL^{-1}) for 0.5 or 4.0 h in the dark. After that, the cells were washed and further stained with HCy-Lyso (10 μM) for 0.5 h. Finally, fluorescence imaging was immediately carried out with an inverted fluorescence microscope.

2.11 Monitoring the change of intracellular ˙OH during ferroptosis

Typically, a total of 2.5×10^3 4T1 cells in 100 μL of culture medium were seeded in each well of the 96-well plate for 24 h of incubation. Then, the cells were pre-treated with erastin (10 μM) or RSL3 (2.0 μM) for 6 h at 37 °C to induce ferroptosis. Subsequently, the growth medium was removed and replaced by

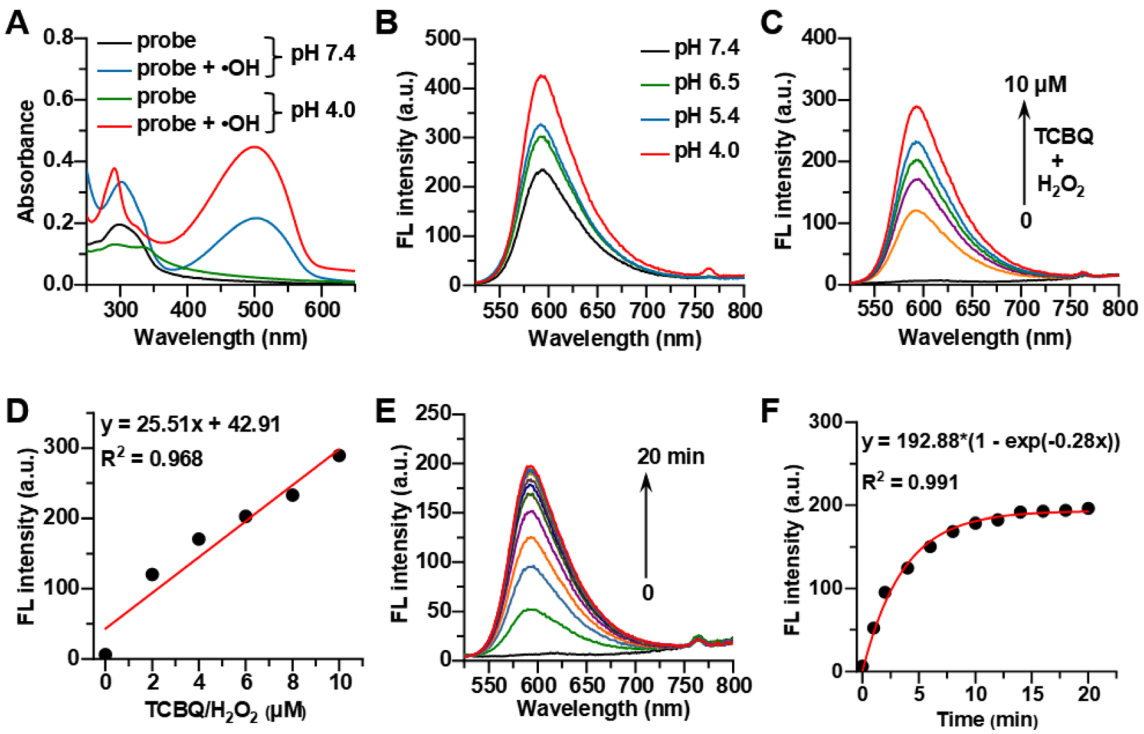

Fig. 1 (A) The UV-vis absorption spectra of 10 μM HCy-Lyso before (black and green) and after (blue and red) response to ˙OH (50 μM TCBQ + 50 μM H_2O_2) in pH 4.0 or 7.4 phosphate buffer solution (10 mM). (B) Fluorescence spectra of 10 μM HCy-Lyso reacting with 50 μM TCBQ/H_2O_2 at different pH conditions. (C) Fluorescence spectra of HCy-Lyso (10 μM) under different concentrations of TCBQ/H_2O_2 (0–10 μM) for 1.0 h in pH 4.0 PBS buffer (10 mM, 37 °C). (D) Linear relationship of fluorescence intensity and TCBQ/H_2O_2 concentration. (E) Time-dependent fluorescence spectra of HCy-Lyso (10 μM) in phosphate buffer solution (10 mM, pH 4.0) upon the addition of 10 μM TCBQ/H_2O_2 at 37 °C for varied times. (F) The corresponding plot of the fluorescence intensity of HCy-Lyso after incubation with TCBQ/H_2O_2 within 20 min. $\lambda_{ex/em}$ = 510/592 nm.

a new culture medium containing 10 μM of HCy-Lyso for 0.5 h for imaging. To inhibit ferroptosis, the cells were incubated with erastin (10 μM) or RSL3 (2.0 μM) in the presence of 10 μM Fer-1. Fluorescence images were collected using an inverted fluorescence microscope.

2.12 Statistical analysis

All experiments were performed 3 times in parallel, and the results were expressed as mean ± standard deviation (S.D.). One-way ANOVA with Tukey's *post hoc* test for multiple comparisons was carried out in GraphPad Prism software version 9.5.0 (GraphPad, San Diego, CA, USA) for statistical analysis. Asterisks indicate significant differences (*P < 0.05, **P < 0.01, ***P < 0.001, ****P < 0.0001).

3 Result and discussion

3.1 Synthesis and spectroscopic property of HCy-Lyso for ˙OH

The hybridization of a subcellular-targeting moiety, specific recognition group, and a suitable fluorophore could afford a platter of highly sensitive and selective probes. Previous studies indicate that the C=N bond in cyanine can be reduced to the C–N bond by $NaBH_4$, which gives rise to the short absorption and emission wavelengths. However, the C–N bond can also be specifically oxidized by ˙OH and converted back to the C=N bond, thus leading to a larger π-conjugation system and "turn-on" fluorescence signals.[52,53] On the basis of this unique feature, we rationally designed and prepared HCy-Lyso, a hybrid of morpholine and hydrocyanine moiety, as a lysosome-targeted fluorescent probe for ˙OH detection. The molecules HCy-Lyso and HCy-OH were synthesized *via* the routes shown in Scheme S1.† Typically, the precursor of HCy-OH could be facilely prepared by a condensation reaction between the indole salt derivatives (compound **1**) and 4-morpholinobenzaldehyde in EtOH solution at 80 °C for 12 h, forming the larger π-conjugation structure with a yield of 56%. According to the reported procedure for this type of reaction, adding a catalytic amount of piperidine or prolonging the reaction time can further increase the reaction yields.[52,54] Subsequently, the C=N bond in indolium moiety was reduced to a C–N bond under $NaBH_4$ in EtOH solution, giving the ˙OH-responsive product of HCy-Lyso in moderate yield. Notably, the type of reaction substrate, amount of $NaBH_4$, and reaction time mainly determine the yield of this reaction.[45,50] All compounds were readily characterized by ^{1}H NMR, ^{13}C NMR, HRMS and IR analytical data (Fig. S5–S12†).

With probe HCy-Lyso in hand, its spectroscopic properties for recognition of ˙OH were tested in a PBS buffer solution (10 mM, 37 °C). The *in vitro* ˙OH was generated by the reaction of tetrachloro-1,4-benzoquinone (TCBQ) and H_2O_2 (a common and efficient way to produce ˙OH).[55] As shown in Fig. 1A, the maximum absorption of HCy-Lyso lies at about 295 nm both in pH 7.4 and 4.0 PBS solution (black and green curves), consistent with its shorter π-conjugation. Upon the addition of TCBQ and

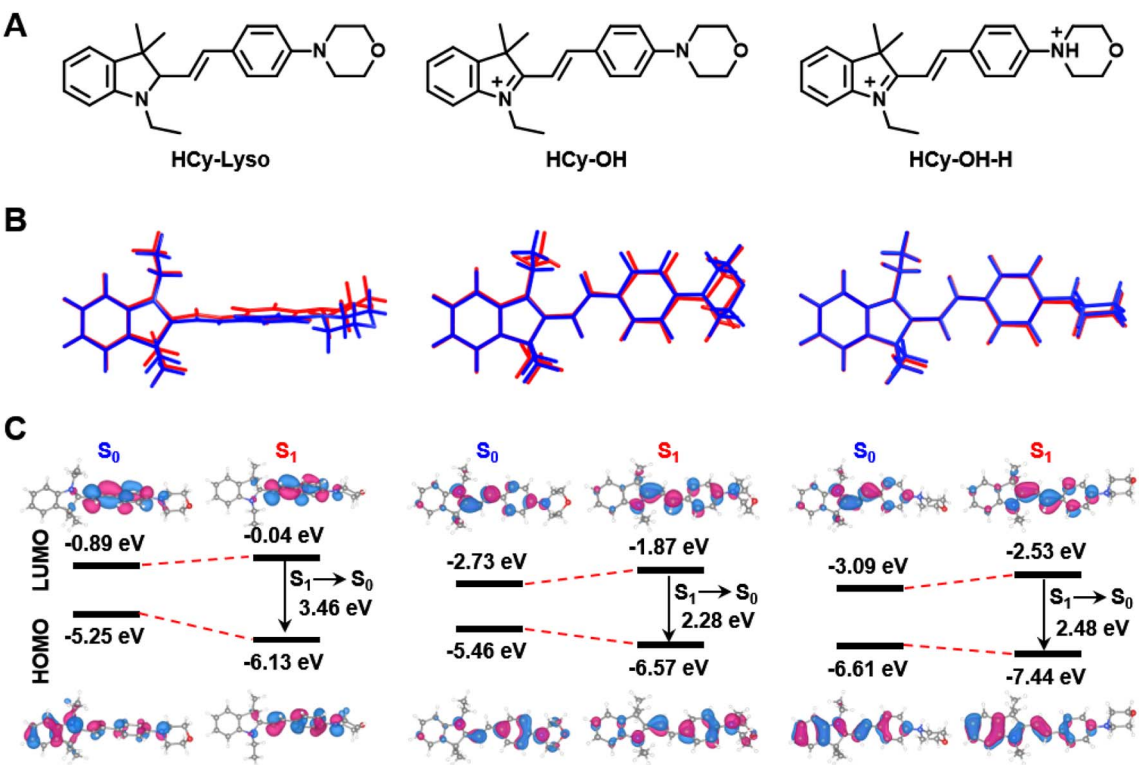

Fig. 2 Molecular structures and theoretical calculation results. (A) Chemical structures of HCy-Lyso, HCy-OH, and HCy-OH-H. (B) Optimized ground state (S_0, blue) and excited state (S_1, red) geometries of all three molecules. (C) Illustration of the frontier molecular orbitals (LUMOs and HOMOs) determined by the B3LYP-D3/6-311G(d) level of theory.

H_2O_2, a new absorption peak appears at 502 nm in pH 7.4 buffer solution (blue curve), implying the hydrogen abstraction of HCy-Lyso to form HCy-OH with larger π-conjugation. Of note, a 2.1-fold absorbance enhancement is observed in pH 4.0 PBS solution (red curve), which is mainly ascribed to a larger π-conjugation system. In fluorescence tests (Fig. 1B), HCy-Lyso also exhibits an obvious pH-dependent fluorescence enhancement in PBS (10 mM, pH 4.0–7.4) solution after the reaction with ˙OH when excited at 510 nm. Lysosomes show an acidic environment (pH 4.0–5.5) in living cells; thus, HCy-Lyso is suitable for detecting lysosomal ˙OH levels. Based on these results, the reaction at pH 4.0 buffer solution was used for the fluorescence response of the probe to ˙OH with different amounts of TCBQ/H_2O_2. As displayed in Fig. 1C, the fluorescence intensity of HCy-Lyso at 592 nm is significantly enhanced with the increase in TCBQ/H_2O_2 concentrations. Meanwhile, a good linear relationship between the fluorescence intensity and the ˙OH concentration is observed from 0 to 10 μM (Fig. 1D). The fluorescence quantum yield (QY) of HCy-Lyso without TCBQ/H_2O_2 is determined as 0.002 in pH 4.0 PBS buffer. However, after the addition of 10 μM TCBQ/H_2O_2, the QY of HCy-Lyso is markedly increased (0.014) and emits a bright fluorescence (Fig. S1†). These results imply the high sensitivity of the probe HCy-Lyso for ˙OH detection. In addition, the time-dependent fluorescence intensity changes at 592 nm of HCy-Lyso were evaluated in pH 4.0 phosphate buffer solution (Fig. 1E). Notably, HCy-Lyso responds rapidly to ˙OH and the fluorescence intensity saturation reaches in a short time (within 20 min), which is essential for monitoring the intracellular ˙OH level (Fig. 1F). Besides, HCy-Lyso also shows excellent selectivity for ˙OH over other common reactive oxygen species (Fig. S2†).

3.2 Theoretical calculation

To gain insights into the proposed principle of probe design, the density functional theory (DFT) and time-dependent density functional theory (TD-DFT) calculations were carried out for HCy-Lyso, HCy-OH, and HCy-OH-H (Fig. 2A). The optimized conformations of all these three molecules were determined with the B3LYP-D3/6-311G(d) level by Gaussian 16 program. As shown in Fig. 2B, the optimized ground-state (S_0) and excited-state (S_1) geometries of HCy-OH and HCy-OH-H show a larger π-conjugation and a more planar molecular configuration, while HCy-Lyso is twisted as the C=N bond is reduced to a C–N bond. For HCy-OH in S_1 geometry, the electron cloud distributed in the highest occupied molecular orbitals (HOMOs) is mostly located on the double-bond bridge ethenyl chain, conjugated benzene ring and morpholine group, while the lowest unoccupied molecular orbitals (LUMOs) are primarily positioned at the C=N bond and benzene ring, resulting in weak fluorescence due to the restricted

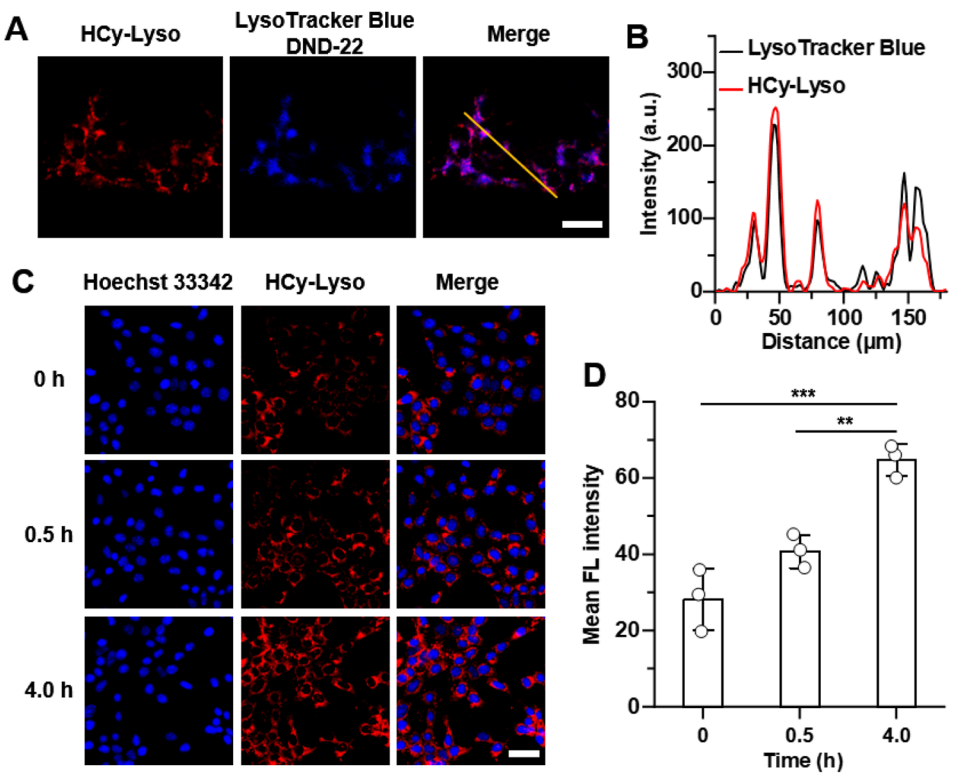

Fig. 3 (A) Colocalization images of 4T1 cells after incubation with 10 μM HCy-Lyso (red channel) and 75 nM LysoTracker Blue DND-22 (blue channel) for 0.5 h. Scale bar: 50 μm. (B) The line-plot graphs exhibit the fluorescence intensity profiles of LysoTracker Blue DND-22 (black) and HCy-Lyso (red) along the yellow dotted lines in the merged fluorescence images from (A). (C) Fluorescence imaging of endogenous ˙OH in 4T1 cells stimulated by PMA. Cells pre-treated with PMA (2.0 μg mL^{-1}) for (a) 0 h, (b) 0.5 h or (c) 4.0 h and then stained with HCy-Lyso (10 μM) for 0.5 h. Scale bar: 50 μm. (D) The relative mean intensity of images from (C). Data are presented as the mean ± SD ($n = 3$). *$P < 0.05$, **$P < 0.01$, ***$P < 0.001$, and ****$P < 0.0001$.

ICT effect. In contrast, HOMOs and LUMOs of HCy-Lyso in S_1 geometry do not distribute on the morpholine unit and exhibit a non-planar structure. It also causes the energy gap from S_0 geometry to rise from 2.73 eV (HCy-OH) to 4.36 eV (HCy-Lyso), consistent with their absorption spectra change (Fig. 2C). More importantly, the HOMOs of the protonation product HCy-OH-H in S_1 geometry are primarily localized along the conjugated chain and cyanine unit except for the benzoindol ring and morpholine group, while the LUMOs are mainly centered at the conjugated ethenyl chain and benzene ring, thus leading to a strong ICT effect. Of note, the emission energy (S_1 to S_0) of HCy-OH-H (2.48 eV) is higher than that of HCy-OH (2.28 eV), indicating that the radiative decay of HCy-OH-H in the excited state is more effective than HCy-OH, thus resulting in stronger fluorescence emission.

3.3 Subcellular location and fluorescence imaging of ˙OH in living cells

By virtue of its excellent performance in an aqueous solution, further experiments were taken to evaluate the applicability of HCy-Lyso in living cells. Initially, the potential cytotoxicity of HCy-Lyso was first measured using a standard CCK-8 assay. As illustrated in Fig. S1,† the cellular viability is still higher than 90% after incubation with a high concentration of HCy-Lyso (10 μM) for 12 h, suggesting the good biosafety of HCy-Lyso. To visualize the cytotoxicity of HCy-Lyso, 4T1 cells treated with various concentrations of HCy- Lyso (0–10 μM) were stained with calcein acetoxymethyl ester (calcein-AM) and propidium iodide (PI) to differentiate dead and viable cells (Fig. S2†). As anticipated, all the groups exhibit strong green fluorescence, while no distinct red fluorescence of PI is observed, even in the high-concentration group. These results demonstrate that HCy-Lyso has good biocompatibility for biological studies. Next, the distribution of HCy-Lyso in living cells was investigated in a colocalization experiment. We can clearly see that the red fluorescence from HCy-Lyso overlaps well with the blue fluorescence of LysoTracker Blue DND-22 with a Pearson's colocalization coefficient of 0.73, indicating that HCy-Lyso can effectively target lysosomes (Fig. 3A and B).

In addition, HCy-Lyso was used to image endogenous ˙OH generated in 4T1 cells under PMA stimuli. As is well known, PMA is an activator of NADPH oxidase (NOX), which can

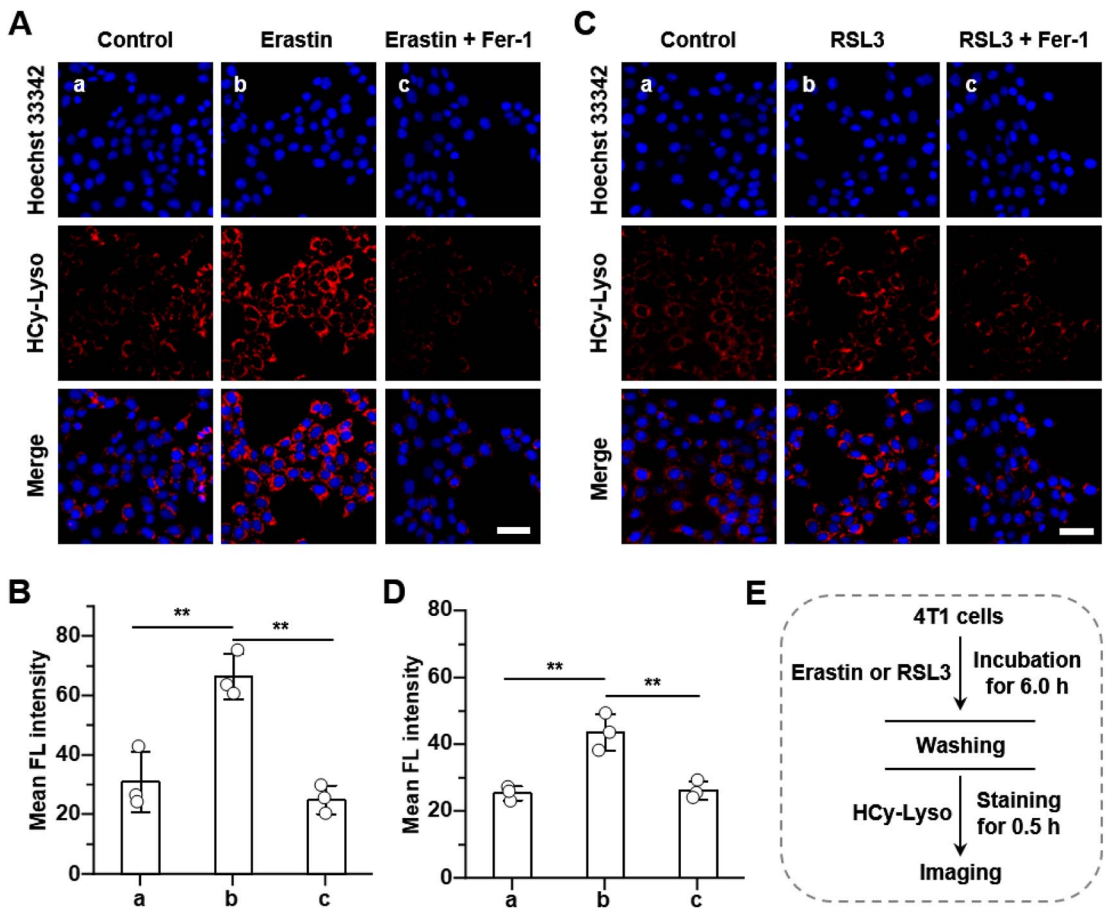

Fig. 4 (A) Fluorescence imaging of ˙OH in 4T1 cells during ferroptosis induced by erastin. (a) Cells only. (b) Cells incubated with erastin (10 μM) for 6.0 h. (c) Cells treated with erastin (10 μM) in the presence of 10 μM Fer-1 for 6.0 h. Scale bar: 50 μm. (B) The relative fluorescence intensity of images (a)–(c) from (A). (C) Fluorescence imaging of ˙OH in 4T1 cells during ferroptosis induced by RSL3. (a) Cells only. (b) Cells incubated with RSL3 (2.0 μM) for 6.0 h. (c) Cells treated with RSL3 (2.0 μM) in the presence of 10 μM Fer-1 for 6.0 h. Scale bar: 50 μm. (D) The relative fluorescence intensity of images (a)–(c) from (C). (E) Schematic procedure for initiation of ferroptosis and staining with HCy-Lyso (10 μM) for imaging. Data are presented as the mean ± SD ($n = 3$). *$P < 0.05$, **$P < 0.01$, ***$P < 0.001$, and ****$P < 0.0001$.

effectively induce the overproduction of intracellular ROS, including ˙OH.[56] As shown in Fig. 3C, upon stimulation with PMA for 0.5 and 4.0 h, the 4T1 cells show a significant time-dependent increase in fluorescence intensity compared to the control group (0 h). Moreover, the mean fluorescence intensity of 4T1 cells treated with a 4.0 h stimulation is 1.6-fold and 3.5-fold higher than cells incubated with PMA for 0.5 and 0 h, respectively (Fig. 3D), suggesting that HCy-Lyso can monitor endogenous ˙OH in living cells.

3.4 Fluorescence imaging of ˙OH generation during ferroptosis

Since ferroptosis is an iron-dependent modality of regulated cell death accompanied by large amounts of ˙OH production, HCy-Lyso was then used to monitor the variation of intracellular ˙OH level triggering by ferroptosis. Initially, 4T1 cells were pre-treated with erastin and (1S, 3R)-RSL3 (RSL3),[57] two representative ferroptosis inducers, to induce the ferroptosis by inhibiting system x_c^- and GPX4 pathways, respectively. As shown in Fig. 4A and E, compared to the control group (image a), the fluorescence intensity of the lysosomes with erastin treatment shows an obvious signal enhancement (image b), indicating the lysosomal ˙OH increase during the ferroptosis process. Conversely, a significant decrease in fluorescence intensity is observed in 4T1 cells treated with erastin in the presence of ferrostatin-1 (Fer-1) (image c), as Fer-1 is a recognized ferroptosis inhibitor that can block the process of ferroptosis. Moreover, the average fluorescence intensity of 4T1 cells incubated with erastin is 2.3-fold and 2.1-fold higher than that of the untreated cells and cells treated with Fer-1, respectively (Fig. 4B). Meanwhile, the group of 4T1 cells incubated with RSL3 also results in a large fluorescence enhancement (1.7-fold), whereas the treatment of Fer-1 shows negligible fluorescence signal (Fig. 4C and D). These results suggest that HCy-Lyso is capable of imaging ˙OH level during different ferroptosis pathways. Erastin is an inducer that exerts its effect primarily by inhibiting the activity of the x_c^- system. As the rate-limiting step in the biosynthesis of GSH is the uptake of cystine *via* the x_c^- system, the inhibitory effect decreases the intracellular cystine levels, followed by inducing ferroptosis. In addition, RSL3 is a GPX4-targeting inducer, which can covalently interact with the selenocysteine site of GPX4, resulting in the upregulation of intracellular LPO and then triggering oxidation-associated ferroptosis. Therefore, HCy-Lyso can be used as a fluorescent probe to indirectly reflect the intracellular cystine level and GPX4 activity through the ˙OH signal during ferroptosis.

4 Conclusion

In summary, a novel lysosome-targeted and ˙OH-responsive fluorescent turn-on probe (HCy-Lyso) has been successfully developed through a molecular engineering strategy for ultra-sensitively monitoring changes in lysosomal ˙OH during ferroptosis. In our approach, the dihydrobenzoindol ring of HCy-Lyso acts as the ˙OH recognition site by virtue of its hydroxylation ability. After reacting with ˙OH, HCy-Lyso can form a large π-conjugation extension, achieving spectral red-shift and obvious fluorescence off–on response at 598 nm. In addition, the morpholine moiety is also introduced to the conjugated core, conferring HCy-Lyso a specific targeting capacity to lysosomes. Of note, the protonation product of HCy-Lyso exhibits a significant fluorescence enhancement after reacting with ˙OH in an acidic environment. HCy-Lyso can be applied for the fluorescence imaging of endogenous ˙OH generated in living cells stimulated by PMA. Moreover, we demonstrate that HCy-Lyso can effectively monitor the variation of lysosomal ˙OH in two ferroptosis-triggering pathways through inhibition of system x_c^- and GPX4. Therefore, this study may offer a new strategy for designing a lysosome-targeted and ˙OH-activated fluorescent probe to detect ˙OH-related physiological and pathological processes.

Conflicts of interest

There are no conflicts to declare.

Acknowledgements

This project was supported by Hainan Province Clinical Medical Center (QWYH202175), Joint project on the Health Science and Technology Innovation of Hainan Province (Grant No. WSJK2024QN104), Natural Science Foundation of China (Grant No. 82060749) and 2022 Health Research Project of Hainan Province (Grant No. 22A200100).

References

1 S. J. Dixon, K. M. Lemberg, M. R. Lamprecht, R. Skouta, E. M. Zaitsev, C. E. Gleason, D. N. Patel, A. J. Bauer, A. M. Cantley, W. S. Yang, B. Morrison III and B. R. Stockwell, *Cell*, 2012, **149**, 1060–1072.
2 B. R. Stockwell, J. P. Friedmann Angeli, H. Bayir, A. I. Bush, M. Conrad, S. J. Dixon, S. Fulda, S. Gascon, S. K. Hatzios, V. E. Kagan, K. Noel, X. Jiang, A. Linkermann, M. E. Murphy, M. Overholtzer, A. Oyagi, G. C. Pagnussat, J. Park, Q. Ran, C. S. Rosenfeld, K. Salnikow, D. Tang, F. M. Torti, S. V. Torti, S. Toyokuni, K. A. Woerpel and D. D. Zhang, *Cell*, 2017, **171**, 273–285.
3 X. Jiang, B. R. Stockwell and M. Conrad, *Nat. Rev. Mol. Cell Biol.*, 2021, **22**, 266–282.
4 J. C. Lv, B. Huo, J. G. Song, Y. H. Xu and S. L. Xie, *J. Multidiscip. Healthc.*, 2022, **15**, 2261–2275.
5 X. T. Wang, Z. X. Wang, J. Gao, Y. L. Dong and Y. X. Chen, *Int. J. Mol. Sci.*, 2021, **22**, 9902–9917.
6 H. F. Yan, T. Zou, Q. Z. Tuo, S. Xu, H. Li, A. Belaidi and P. Lei, *Signal Transduction Targeted Ther.*, 2021, **6**, 49–64.
7 H. B. Fang, Y. C. Chen, S. S. Geng, S. K. Yao, Z. J. Guo and W. J. He, *Anal. Chem.*, 2022, **94**, 17904–17912.
8 C. Liang, X. Zhang, M. Yang and X. Dong, *Adv. Mater.*, 2019, **31**, e1904197.
9 H. Li, W. Shi, X. Li, Y. Hu, Y. Fang and H. Ma, *J. Am. Chem. Soc.*, 2019, **141**, 18301–18307.
10 H. Wang, Y. Cheng, C. Mao, S. Liu, D. Xiao, J. Huang and Y. Tao, *Mol. Ther.*, 2021, **29**, 2185–2208.

11 O. Marques, B. M. da Silva, G. Porto and C. Lopes, *Cancer Lett.*, 2014, **347**, 1–14.
12 S. Piao and R. K. Amaravadi, *Ann. N. Y. Acad. Sci.*, 2016, **1371**, 45–54.
13 H. Huang, B. Yu, P. Zhang, J. Huang, Y. Chen, G. Gasser, L. Ji and H. Chao, *Angew. Chem., Int. Ed.*, 2015, **54**, 14049–14052.
14 A. Ballabio, *EMBO Mol. Med.*, 2016, **8**(2), 73–76.
15 C. Settembre, A. Fraldi, D. L. Medina and A. Ballabio, *Nat. Rev. Mol. Cell Biol.*, 2013, **14**(5), 283–296.
16 C. Watts, *Biochim. Biophys. Acta*, 2012, **1824**, 14–21.
17 J. Camakaris, I. Voskoboinik and J. F. Mercer, *Biochem. Biophys. Res. Commun.*, 1999, **261**(2), 225–232.
18 T. Nevitt, H. Ohrvik and D. J. Thiele, *Biochim. Biophys. Acta, Mol. Cell Res.*, 2012, **1823**(9), 1580–1593.
19 Y. F. Wang, V. Hodgkinson, S. Zhu, G. A. Weisman and M. J. Petris, *Adv. Nutr.*, 2011, **2**(2), 129–137.
20 S. Lutsenko, *Curr. Opin. Chem. Biol.*, 2010, **14**(2), 211–217.
21 H. Y. Tang, H. Y. Huang, D. Wang, P. Li, Z. Y. Tian, D. J. Li, S. M. Wang, R. L. Ma, T. Xia and A. G. Wang, *J. Hazard. Mater.*, 2022, **430**, 128483–128497.
22 F. Rizzollo, S. More, P. Vangheluwe and P. Agostinis, *Trends Biochem. Sci.*, 2021, **46**, 960–975.
23 M. Mauthe, I. Orhon, C. Rocchi, X. D. Zhou, M. Luhr, K. J. Hijlkema, R. P. Coppes, N. Engedal, M. Mari and F. Reggiori, *Autophagy*, 2018, **14**, 1435–1455.
24 W. Li, S. L. Yin, Y. Shen, H. Y. Li, L. Yuan and X. B. Zhang, *J. Am. Chem. Soc.*, 2023, **145**, 3736–3747.
25 K. Pierzynowska, E. Rintz, L. Gaffke and G. Węgrzyn, *Cell*, 2021, **10**, 365–387.
26 X. D. Lv, W. F. Tang, J. J. Qin, W. Q. Wang, J. C. Dong and Y. Wei, *Front. Immunol.*, 2023, **14**, 1140791–1140810.
27 J. D. Mancias, X. Wang, S. P. Gygi, J. W. Harper and A. C. Kimmelman, *Nature*, 2014, **509**, 105–109.
28 M. Ghosh, F. Carlsson, A. Laskar, X. M. Yuan and W. Li, *FEBS Lett.*, 2011, **585**, 623–629.
29 W. Bao, M. Liu, J. Meng, S. Liu, S. Wang, R. Jia, Y. Wang, G. Ma, W. Wei and Z. Tian, *Nat. Commun.*, 2021, **12**, 6399.
30 S. R. Bonam, F. Wang and S. Muller, *Nat. Rev. Drug Discovery*, 2019, **18**, 923–948.
31 X. Li, X. Gao, W. Shi and H. Ma, *Chem. Rev.*, 2014, **114**, 590–659.
32 D. Liu, Z. He, Y. Zhao, Y. Yang, W. Shi, X. Li and H. Ma, *J. Am. Chem. Soc.*, 2021, **143**, 17136–17143.
33 N. Ding, Z. Li, X. Tian, J. Zhang, K. Guo and P. Wang, *Chem. Commun.*, 2019, **55**, 13172–13175.
34 Y. Zhang, X.-F. Zhang, Q. Chen, X.-Q. Cao and S.-L. Shen, *Sens. Actuators, B*, 2022, **353**, 131145.
35 J. Zhou, B. Jiang, C. Gao, K. Zhu, W. Xu and D. Song, *Sens. Actuators, B*, 2022, **355**, 131310.
36 Y. Feng, G. Nie, W. Liang, W. Li, Y. Zhang, K. Wang and D. Chen, *Sens. Actuators, B*, 2022, **355**, 131285.
37 B. Chen, S. Mao, Y. Sun, L. Sun, N. Ding, C. Li and J. Zhou, *Chem. Commun.*, 2021, **57**, 4376–4379.
38 X. Bai, Y. Huang, M. Lu and D. Yang, *Angew. Chem., Int. Ed.*, 2017, **56**, 12873–12877.
39 L. Chen, X. Wu, H. Yu, L. Wu, Q. Wang, J. Zhang, X. Liu, Z. Li and X.-F. Yang, *Anal. Chem.*, 2021, **93**, 14343–14350.
40 X. Wang, P. Li, Q. Ding, C. Wu, W. Zhang and B. Tang, *Angew. Chem., Int. Ed.*, 2019, **58**, 4674–4678.
41 X. Jiao, Y. Li, J. Niu, X. Xie, X. Wang and B. Tang, *Anal. Chem.*, 2018, **90**, 533–555.
42 L. Yuan, W. Lin and J. Song, *Chem. Commun.*, 2010, **46**, 7930–7932.
43 L. Zeng, T. Xia, W. Hu, S. Chen, S. Chi, Y. Lei and Z. Liu, *Anal. Chem.*, 2018, **90**, 1317–1324.
44 Y. Chen, Z. Hu, M. Yang, J. Gao, J. Luo, H. Li and Z. Yuan, *Sens. Actuators, B*, 2022, **362**, 131742.
45 Y. An, X. Luo, S. Wei, J. Lv, J. Gao, X. Li, M. Yang, J. Luo, Y. Wu, G. Wei, Z. Yuan and H. Li, *Sens. Actuators, B*, 2023, **397**, 134653.
46 L.-L. Wang, Y.-Z. Mai, M.-H. Zheng, X. Wu and J.-Y. Jin, *Sens. Actuators, B*, 2022, **373**, 132707.
47 X. Xia, C. Shi, S. He, R. Wang, Z. Zhang, Y. Hu, J. Cao, T. Liu, D. Zhou, W. Sun, J. Fan and X. Peng, *Adv. Funct. Mater.*, 2023, **33**, 2300340.
48 S. Cai, R. Guo, Q. Liu, X. Gong, X. Li, Y. Yang and W. Lin, *New J. Chem.*, 2022, **46**, 8171.
49 Q.-T. Liao, J.-J. Chao, W.-X. Wang, T. Liu, G.-J. Mao, F. Xua and C.-Y. Li, *Chem. Commun.*, 2023, **59**, 5607.
50 A. D. Becke, *J. Chem. Phys.*, 1993, **98**, 5648–5652.
51 M. J. Frisch, G. W. Trucks, H. B. Schlegel, G. E. Scuseria, M. A. Robb, J. R. Cheeseman, G. Scalmani, V. Barone, G. A. Petersson, H. Nakatsuji, X. Li, M. Caricato, A. V. Marenich, J. Bloino, B. G. Janesko, R. Gomperts, B. Mennucci, H. P. Hratchian, J. V. Ortiz, A. F. Izmaylov, J. L. Sonnenberg, D. Williams-Young, F. Ding, F. Lipparini, F. Egidi, J. Goings, B. Peng, A. Petrone, T. Henderson, D. Ranasinghe, V. G. Zakrzewski, J. Gao, N. Rega, G. Zheng, W. Liang, M. Hada, M. Ehara, K. Toyota, R. Fukuda, J. Hasegawa, M. Ishida, T. Nakajima, Y. Honda, O. Kitao, H. Nakai, T. Vreven, K. Throssell, J. A. Montgomery Jr, J. E. Peralta, F. Ogliaro, M. J. Bearpark, J. J. Heyd, E. N. Brothers, K. N. Kudin, V. N. Staroverov, T. A. Keith, R. Kobayashi, J. Normand, K. Raghavachari, A. P. Rendell, J. C. Burant, S. S. Iyengar, J. Tomasi, M. Cossi, J. M. Millam, M. Klene, C. Adamo, R. Cammi, J. W. Ochterski, R. L. Martin, K. Morokuma, O. Farkas, J. B. Foresman, and D. J. Fox, *Gaussian 16*, Gaussian, Inc, Wallingford CT, 2019.
52 Y. Chen, Z. Hu, M. Yang, J. Gao, J. Luo, H. Li and Z. Yuan, *Sens. Actuators, B*, 2022, **362**, 131742.
53 H. Li, Y. An, X. Luo, J. Gao, M. Yang, X. Li, X. Li, W. Shi, Z. Yuan and H. Ma, *Chem. Eng. J.*, 2023, **476**, 146749.
54 C. Xiang, C. Li, J. Xiang, Y. Luo, J. Peng, G. Deng, J. Wang, S. Kolemen, H. Li, P. Zhang, P. Gong and L. Cai, *Mater. Chem. Front.*, 2021, **5**, 7638.
55 B.-Z. Zhu, B. Kalyanaraman and G.-B. Jiang, *Proc. Natl. Acad. Sci. U. S. A.*, 2007, **104**, 17575–17578.
56 D. Jagnandan, J. E. Church, B. Banfi, D. J. Stuehr, M. B. Marrero and D. J. R. Fulton, *J. Biol. Chem.*, 2007, **282**, 6494–6507.
57 W. S. Yang, R. SriRamaratnam, M. E. Welsch, K. Shimada, R. Skouta, V. S. Viswanathan, J. H. Cheah, P. A. Clemons, A. F. Shamji, C. B. Clish, L. M. Brown, A. W. Girotti, V. W. Cornish, S. L. Schreiber and B. R. Stockwell, *Cell*, 2014, **156**, 317–331.